The Journal of Chemical Physics

Characterization of the interface of binary mixed DOPC:DOPS liposomes in water: The impact of charge condensation

Cite as: J. Chem. Phys. **146**, 044701 (2017); https://doi.org/10.1063/1.4974084
Submitted: 21 October 2016 . Accepted: 27 December 2016 . Published Online: 25 January 2017

Cornelis Lütgebaucks, Carlos Macias-Romero, and Sylvie Roke

AIP Publishing

Characterization of the interface of binary mixed DOPC:DOPS liposomes in water: The impact of charge condensation

Cornelis Lütgebaucks, Carlos Macias-Romero, and Sylvie Roke[a)]
Laboratory for fundamental BioPhotonics (LBP), Institute of Bioengineering (IBI), and Institute of Materials Science (IMX), School of Engineering (STI), and Lausanne Centre for Ultrafast Science (LACUS), École Polytechnique Fédérale de Lausanne (EPFL), CH-1015 Lausanne, Switzerland

(Received 21 October 2016; accepted 27 December 2016; published online 25 January 2017)

Solutions of liposomes composed of binary mixtures of anionic dioleoylphosphatidylserine (DOPS) and zwitterionic dioleoylphosphatidylcholine (DOPC) are investigated with label-free angle-resolved (AR) second harmonic scattering (SHS) and electrophoretic mobility measurements. The membrane surface potential is extracted from the AR-SHS response. The surface potential changes from −10 to −145 mV with varying DOPS content (from 0% to 100%) and levels off already at ∼10% DOPS content. The ζ-potential shows the same trend but with a drastically lower saturation value (−44 mV). This difference is explained by the formation of a condensed layer of Na^+ counterions around the outer leaflet of the liposome as predicted by charge condensation theories for polyelectrolyte systems.
[http://dx.doi.org/10.1063/1.4974084]

I. INTRODUCTION

Lipid bilayer membranes are primary building blocks of organisms. These membranes exhibit a diverse composition in order to separate functional compartments and to control signalling processes. In plasma membranes, the lipid composition between the two leaflets is highly asymmetric and changes dynamically to trigger environmental responses. For instance, cells that undergo apoptosis increase the concentration of anionic phosphatidylserine (PS) in the outer leaflet of the plasma membrane to signal phagocytes to approach and digest them, whereas in healthy cells, PS lipids are only present in the inner leaflet.[1]

In order to understand the membrane structure, hydration, and the changes therein, it is crucial to characterize the interfacial properties of lipid membranes and their aqueous environment. Non-resonant second harmonic scattering[2,3] (SHS) is an optical process used to measure the net orientational order of water molecules along the surface normal of particles,[4,5] droplets,[6–8] or liposomes.[9,10] Polarization- and angle-resolved (AR) SHS were recently demonstrated as a method to obtain a unique value for the surface potential of a particle in aqueous solution.[11] Key to this method is the fact that the nonlinear polarization of water at the second harmonic frequency depends linearly on the ensemble electrostatic field in the solution. This ensemble electrostatic field originates from all charges and partial charges (such as dipoles and quadrupoles) in the solution. The integral of this field from the surface of the particle into the bulk of the solution (considered as infinity) constitutes the surface potential.[12] Polarization resolved AR-SHS can be described by a set of exact analytical expressions[13] that rely on the surface potential and one non-vanishing surface susceptibility tensor element that describes the orientational order of water at the interface. Combined AR-SHS and sum-frequency scattering (SFS) studies[10] were recently used to probe the transmembrane asymmetry in single component anionic DOPS and zwitterionic DOPC liposomes, as well as liposomes composed of a 1:1 mixture of DOPC and DOPS. DOPC and DOPS are two of the main constituents of the eukaryotic plasma membrane.[14] The structures are sketched in Fig. 1(a). Under pH neutral conditions, they are either charged (DOPS, −1) or neutral (DOPC). It was found that the molecular transmembrane asymmetry of the three systems originates from a disparity in the amount of hydrating water molecules that surround the phospholipid head groups. In contrast, transmembrane asymmetry in the form of a different number of lipid molecules in the inner and outer leaflets was absent for liposomes composed of DOPC, DOPS, or a 1:1 mixture of DOPC:DOPS.[10]

In this work, we further quantify the surface properties of liposomes in water that are composed of a binary mixture of DOPC and DOPS. We apply AR-SHS and electrophoretic mobility measurements to dilute solutions of liposomes composed of different binary mixtures of DOPS and DOPC, spanning the full range of possible mixtures. The membrane surface potential is extracted from the polarization resolved AR-SHS response. Upon increasing the amount of DOPS in the membrane from 0% to 100%, the surface potential changes from −10 ± 20 mV to −145 ± 30 mV and levels off at ∼10% DOPS content. The ζ-potential values derived from the electrophoretic mobility measurements show the same trend but with a drastically lower saturation value (−44 mV). This

a)Author to whom correspondence should be addressed. Electronic mail: sylvie.roke@epfl.ch

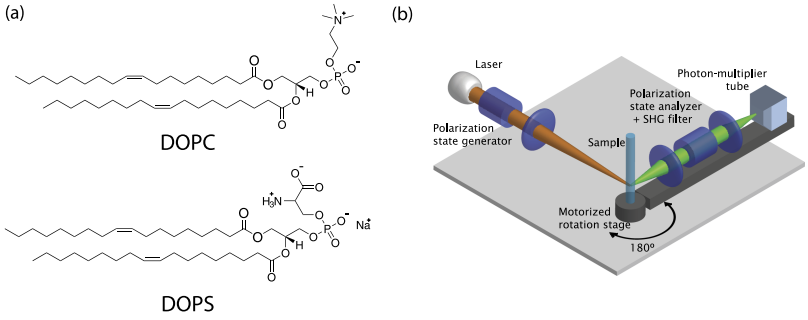

FIG. 1. Lipid structure and second harmonic setup. (a) Molecular structure of zwitterionic DOPC and an anionic DOPS. (b) Sketch of the second harmonic scattering setup.

observation is explained by the formation of a condensed layer of Na^+ counter-ions around the outer leaflet of the liposome and agrees with the predictions of charge condensation theory for polyelectrolyte systems.

II. MATERIALS AND METHODS

A. Materials

All chemicals were used as received. Sulfuric acid (95%–97%, ISO) and chloroform (Emsure, ACS, ISO) were purchased from Merck (Germany) and hydrogen peroxide (30%) from Reactolab SA (Switzerland). Sodium chloride (NaCl, >99%), phosphorus standard solution (0.6 M), L-ascorbic acid (ACS, ≥99%), ammonium molybdate (VI, ACS, 81%–83%), and ammonium hydroxide (30%) were purchased from Sigma-Aldrich Switzerland. 1,2-dioleoyl-*sn*-glycero-3-phosphocholine (DOPC) and 1,2-dioleoyl-*sn*-glycero-3-phospho-L-serine (sodium salt) (DOPS) and dioleoyl-*sn*-glycero-3-phospho-(1′rac-glycerol) were purchased in powder form (>99%) from Avanti Polar Lipids (Al, USA) and stored at −20 °C.

B. Cleaning procedure

Glassware was cleaned with a 1:3 H_2O_2:H_2SO_4 solution and rinsed with ultrapure water (Milli Q, Merck Millipore, Inc., electrical resistance of 18.2 MΩ cm). The glassware that was used for the determination of the phosphorus content was cleaned according to a two-step cleaning procedure: here, a primary cleaning with a 100 °C 3:1:1 H_2O:H_2SO_4:H_2O_2 solution was applied, followed by a cleaning with an 80 °C 3:1:1 H_2O:NH_4OH_4:H_2O_2 solution. In between and after the cleaning, the glassware was rinsed with ultrapure water.

C. Liposome preparation

Lipid stock solutions were created by dissolving lipid powder in chloroform using 4 ml screwcap glass vials. Stocks were stored at −20 °C, for a maximum period of 3 month. To create liposomes, the respective quantities of lipid stock solutions were pipetted into a round-bottom glass tube using a glass syringe (Hamilton). For mixed liposomes, the different lipid stock solutions were mixed together in the glass tube. The chloroform was evaporated from the glass tube under constant rotation using a gentle stream of N_2 gas. The residual chloroform that remained in the formed lipid film was evaporated by keeping it under room temperature vacuum (<100 mbar, created by an oil-free diaphragm pump) for at least 1.5 h. To form multilamellar vesicles, 1 ml of ultrapure water was added to the tubes that were then vigorously shaken. The room temperature multilamellar vesicle solutions were placed in a Mini extruder (Avanti Polar Lipids) together with a 100 nm diameter polycarbonate membrane. The solutions were pushed 51 times through the membrane to form unilamellar vesicles. The obtained liposome solutions were diluted with varying amounts of water or NaCl solutions to obtain the desired liposome concentration prior to the measurements. The unilamellar vesicles were stored up to 2 weeks at 4 °C. The quality of the liposomes was checked by dynamic light scattering (DLS) and electrophoretic mobility measurements at 24 °C (using a Malvern ZS nanosizer) after extrusion and before each experiment.

D. Liposome characterization

The size distribution of the liposomes was determined in three subsequent measurements, 11 runs each, by means of DLS. The ζ-potential of the liposomes was determined by measuring the electrophoretic mobility in three subsequent measurements, each 75 runs at automated voltage, and converting the mobility values into ζ-potential values using the Smoluchowski approximation.[15] The liposomes were consistently found to have a mean diameter of ∼100 nm with a polydispersity index (PDI) of less than 0.1. The lipid concentration in the samples was evaluated by a colorimetric assay (described in detail in Ref. 16) determining the total phosphorus content. The lipid concentration was 0.5 mg lipids/ml (*w*/*w*) for dynamic light scattering (DLS), ζ-potential measurements, and SHS experiments. SHS measurements were performed at 24 °C. pH measurements of the DOPS liposome solution were carried out in triplet using a pH meter (Hanna, HI 5522). The results of the characterization of all samples are given in Table I.

E. Second harmonic scattering

Polarization resolved AR-SHS measurements were performed using the same setup as described in Ref. 19. Figure 1(b) shows a schematic of the setup. Briefly, a 174 fs pulsed laser beam (average power 60 mW) with a center wavelength of 1032 nm and a repetition rate of 200 kHz was focused into a cylindrical glass sample cell (4.2 mm inner diameter, high precision cylindrical glass cuvettes, LS instruments, Switzerland). The input-polarization was controlled by a Glan-Taylor polarizer (GT10-B, Thorlabs, Germany) and a zero-order half wave plate (WPH05M-1030). The frequency content of the fundamental beam was controlled with a long pass filter (FEL0750, Thorlabs) before the beam was focused.

TABLE I. Sample characterization and input parameters used in Eqs. (2) and (3).

Parameters\ Liposomes:	DOPC	PC:PS [9:1]	PC:PS [8:2]	PC:PS [7:3]	PC:PS [6:4]	PC:PS [5:5]	DOPS
Hydrodynamic radius (nm)	47	56	56.9	57.5	58.4	57.6	59
Head group area (nm^2)	0.725[a]	0.71	0.71	0.7	0.696	0.689	0.65[a]
Number density (N_p) × 10^{12} (#/ml)	3.3	3.59	3.43	3.23	2.92	3.21	2.87
SH wavelength (vacuum) (nm)	514	514	514	514	514	514	514
Temperature (°C)	24	24	24	24	24	24	24
Liposome inner refractive index (n_p, 514 nm)	1.4[b]	1.4[b]	1.4[b]	1.4[b]	1.4[b]	1.4[b]	1.4[b]
Refractive index solution (n_{H_2O}, 514 nm)	1.33	1.33	1.33	1.33	1.33	1.33	1.33
Ionic strength (mM)	0.0022	0.092	0.138	0.148	0.141	0.121	0.246
$\chi_2^{(3)} \cdot 10^{-21}$ (m^2/V^2)	1.03	1.03	1.03	1.03	1.03	1.03	1.03

[a]Taken from Ref. 17.
[b]Adapted from Ref. 18.

The beam waist at the focus was 36 μm ($2w_0$) and the corresponding Rayleigh length was ~0.94 mm. The scattered SH light was collected and collimated with a plano-convex lens (f = 5 cm), passed through an iris with variable diameter, analyzed (using a Glan Taylor polarizer (GT10-A, Thorlabs), and filtered (ET525/50, Chroma Technologies, VT, USA) before being focused into a gated photomultiplier tube (H7421-40, Hamamatsu Photonics, France). The acceptance angle was set to 3.4° by controlling the diameter of the iris. Patterns were obtained in steps of 5° from $\theta = -90°$ to $\theta = 90°$ with 0° being the forward direction of the fundamental beam. The obtained SHS intensity of the liposome solutions is reduced by the SHS from a liposome free solution collected in the same polarization combination to correct for Hyper-Rayleigh scattering through the bulk solution. The thus obtained response is normalized by the isotropic uncorrelated (SSS) SHS from ultrapure water,

$$S_{Pii}(\theta) = \frac{I(\theta)_{SHS,liposomes,Pii} - I(\theta)_{SHS,solution,Pii}}{I(\theta)_{SHS,solution,SSS}}, \qquad (1)$$

where *ii* is a placeholder for the polarization of the incoming beams that is either P (parallel to the scattering plane) or S (vertical to the scattering plane) polarized light. Data points were acquired using 20 × 1.5 s acquisition times with a photomultiplier gate width of 10 ns.

F. Determining the surface potential

Using nonlinear light scattering theory, we previously devised a set of equations, described in detail in Refs. 11 and 13, that allows us to extract a unique value of the surface potential without making any assumptions about the surface chemistry. The equations used to obtain the surface potential are derived from the nonlinear light scattering theory using the Rayleigh-Gans-Debye-(RGD) approximation with a first-order correction for the jump in the electromagnetic field amplitude across the interface.[20,21] The amplitude of the scattered polarized electromagnetic field is a function of the geometry of the illuminating electromagnetic fields and their respective polarization state, the shape and size of the particles, and the effective nonlinear particle susceptibility, a material property. Within the RGD approximation, analytical solutions[12] are obtained for SHS from a sphere (or shell). They are as follows:

$$\frac{I_{PPP}(\theta)}{I_{SSS}(\theta)} = \frac{\left(E_P(\omega)^2\left[\cos\left(\frac{\theta}{2}\right)^3 \Gamma_1^{(2)} + \cos\left(\frac{\theta}{2}\right)\left(\Gamma_2^{(2)} + \Gamma_2^{(3)'}\right)(2\cos(\theta)+1)\right]\right)^2}{\bar{\mu}^2 N_b/N_p} = S_{PPP}(\theta) \qquad (2)$$

TABLE II. Analytical expressions used for computing Eqs. (2) and (3) comprised of the surface and effective particle susceptibility elements of the interface and the diffuse double layer, the form factor functions, and the scattering vector.

Surface and particle Susceptibility elements[13,24]	Form factor functions and scattering vector[13,21]
$\chi_{s,1}^{(2)''} = 27\eta \frac{\left(\chi_{s,1}^{(2)}\eta^2 + 3\chi_{s,2}^{(2)}(\eta^2-1)\right)}{(2+\eta)^3}, \quad \eta = \left(\frac{n_p}{n_{H_2O}}\right)^2$	$F_1(qR) = 2\pi R^2 i\left(\frac{\sin(qR)}{(qR)^2} - \frac{\cos(qR)}{qR}\right)$
$\chi_{s,2}^{(2)''} = 27\eta \frac{\chi_{s,2}^{(2)}}{(2+\eta)^3}$	$F_2(qR) = 4\pi R^2 i\left(3\frac{\sin(qR)}{(qR)^4} - 3\frac{\cos(qR)}{(qR)^3} - \frac{\sin(qR)}{(qR)^2}\right)$
$\chi_2^{(3)''} = 27\eta \frac{\chi_2^{(3)'}}{(2+\eta)^3}, \quad \chi_2^{(3)'} = \frac{N_b}{\varepsilon_0}\left(\bar{\beta}^{(3)} + \frac{\bar{\beta}^{(2)}\mu_{dc}}{3k_B T}\right)$	$F_3(\kappa R, qR) = 2\pi R^2 i \frac{qR\cos(qR) + \kappa R \sin(qR)}{(qR)^2 + (\kappa R)^2}$
$\Gamma_1^{(2)} = (2F_1(qR) - 5F_2(qR))\chi_{s,1}^{(2)''}$	$\boldsymbol{q} \equiv \boldsymbol{k}_0 - 2\boldsymbol{k}_1, \quad q = \left\lvert\frac{4\pi n_{H_2O}}{\lambda_{SH}} \sin\frac{\theta}{2}\right\rvert$
$\Gamma_2^{(2)} = F_2(qR)\chi_{s,1}^{(2)''} + 2F_1(qR)\chi_{s,2}^{(2)''}$	
$\Gamma_2^{(3)'} = 2\chi_2^{(3)''}\Phi_0(F_1(qR) + F_3(qR,\kappa R))$	

and

$$\frac{I_{PSS}(\theta)}{I_{SSS}(\theta)} = \frac{\left(E_S(\omega)^2\left[\cos\left(\frac{\theta}{2}\right)\left(\Gamma_2^{(2)} + \Gamma_2^{(3)'}\right)\right]\right)^2}{\bar{\mu}^2 N_b/N_p} = S_{PSS}(\theta), \quad (3)$$

where $\Gamma_i^{(2)}$ and $\Gamma_2^{(3)'}$ are the only non-zero elements of the nonlinear effective particle susceptibilities (defined in Ref. 22), $\bar{\mu} = \bar{\beta}^{(2)}_{H_2O} E(\omega)^2$, the averaged induced second-order dipole moment with $\bar{\beta}^{(2)}_{H_2O}$ the averaged hyperpolarizability of water; N_p is the number of liposomes and N_b is the density of bulk water ($3.34 \cdot 10^{28}$ molecules/m^3). The elements of the nonlinear effective particle susceptibility are linked to the surface susceptibility according to the expressions in Table II. N_b/N_p is the number of bulk water molecules per liposome. Water, the main phase, with a known[23] nonlinear optical response, is used here as a reference. The non-zero second-order susceptibility element $\chi_2^{(2)} = 1.36 \times 10^{-22}$ (m^2/V) was kept fixed since the value does not significantly differ between pure DOPC and DOPS liposomes.[11] Other required experimental parameters, constants, and equalities are listed for completeness in Tables I and III.

Equations (2) and (3) are derived assuming that the liquid interface is spatially isotropic in the azimuthal direction, the optical process is lossless, and that water possesses a broad orientational distribution. These assumptions were validated in previous studies.[11,13,25] Although we employ the RGD assumption for the linear interaction, the nonlinear interaction contains a correction to account for the change in field amplitude when the optical electromagnetic fields cross the particle/water interface. Dadap *et al.* showed that a linear correction term to the second-order susceptibility is sufficient to correct for the change in the electromagnetic field when it crosses the interface.[24] This correction for the susceptibility value is used here and listed in Table II.

Another assumption is the absence of multiple scattering, which depends on the size and refractive index mismatch between the bulk of the particles and the liquid medium. Schneider *et al.* showed that this is typically the case for the concentrations used here.[2] Since liposomes are shells that contain water, we expect that the RGD theory is in this case exact and that multiple scattering does not occur in contrast to polystyrene particles. To verify this last assumption, we compared the scattering intensities of samples with

TABLE III. Constants and equalities as used in Eqs. (2) and (3) to describe the water normalized scattering patterns.

Constants and equalities
$\mu_{dc} = 8.97 \times 10^{-30}$ Cm[23]
$\bar{\beta}^{(2)} = 3.09 \times 10^{-52}$ C^{3}m^{3}J^{-2} [23]
$\bar{\beta}^{(3)} = 4.86 \times 10^{-62}$ C^{4}m^{4}J^{-3} [23]
$\chi^{(2)}_{s,1} = \chi^{(2)}_{s,\perp\perp\perp} - \chi^{(2)}_{s,\parallel\parallel\perp} - \chi^{(2)}_{s,\parallel\perp\parallel} - \chi^{(2)}_{s,\perp\parallel\parallel}$
$\chi^{(2)}_{s,2} = \chi^{(2)}_{s,\parallel\parallel\perp}$($\perp$ surface normal direction; $\parallel$ tangential direction)
$\chi^{(2)}_{s,1} \to 0$
$\chi^{(2)}_{s,4} = \chi^{(2)}_{s,3} = \chi^{(2)}_{s,2}$, $\chi_4^{(3)'} = \chi_3^{(3)'} = \chi_2^{(3)'}$
$\chi_2^{(3)'} = 10.3 \times 10^{-22}$ m^2/V^2(calculated from $\bar{\beta}^{(3)}$)

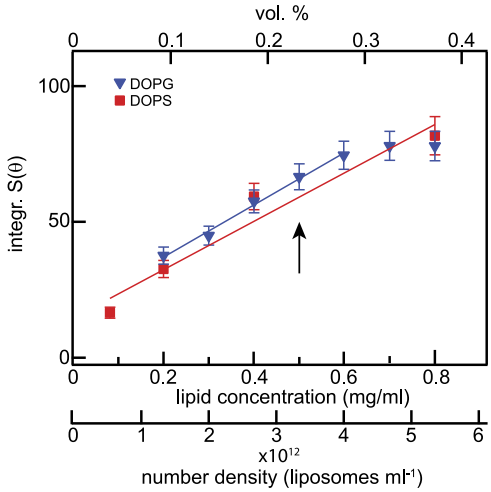

FIG. 2. Integrated SHS response relative to that of water as a function of liposome concentration. Concentration dependence of the integrated PPP SHS signal for anionic liposomes.

different liposome concentrations. Figure 2 shows the integrated S(θ) response over a scattering angle range from −90° to 90° using the PPP polarization combination for two different anionic liposome solutions (composed of DOPS or dioleolyphosphatidyl-1′-*rac*-glycerol (DOPG), both extruded through 100 nm pores) in ultrapure water. The error bar represents the angle-integrated standard deviation from 20 measurements per angle. It can be seen that the SH intensity increases linearly for both samples, but possibly saturates at ∼4.68×10^{12} liposomes/ml (∼0.7 mg/ml). At this concentration, the inter-liposome distance from membrane to membrane is ∼500 nm for both samples, comparable to the second harmonic wavelength, suggesting the onset of nonlinearity of the scattered intensity as a function of liposome concentration. In order to avoid such effects, all measurements were performed using ∼3.3×10^{12} liposomes/ml (0.5 mg/ml).

III. RESULTS AND DISCUSSION

Figures 3(a) and 3(b) show the measured SH scattered intensity from liposomes composed of three different DOPC:DOPS ratios as a function of scattering angle θ for the two independent polarization combinations (PPP and PSS). Figure 3(c) shows the maximum scattered intensity (at θ = 50°) as a function of DOPS content (*w*/*w* %) in the liposome. The SH intensity that is directly linked to the orientational order of interfacial water molecules[13] can be seen to increase with increasing amount of DOPS molecules in the membrane and saturates at ∼10% (*w*/*w*) DOPS content.

To understand the saturation behavior in more detail, we analyzed the data in Figs. 3(a) and 3(b) following the above mentioned method and extracted unique surface potential values from the polarimetric AR-SHS data. The solid lines in Figs. 3(a) and 3(b) represent fits to the nonlinear light scattering equations (Eqs. (2) and (3), using the input parameters of Table I) are the surface susceptibility element $\chi^{(2)}_{s,2} = 1.36(\pm 0.2) \cdot 10^{-22}$ m^2/V with surface potential values in the range from $\Phi_0 = -10 \pm 20$ mV (pure DOPC) to

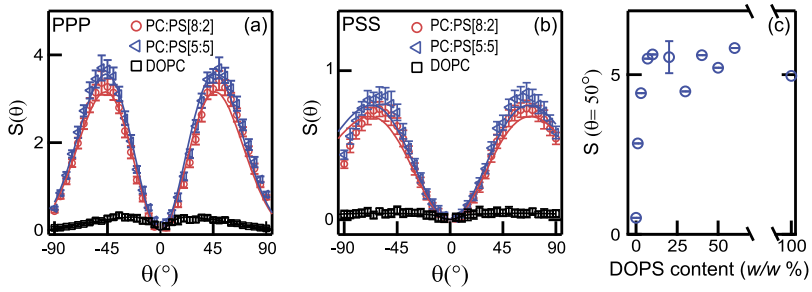

FIG. 3. Polarized AR-SHS patterns from liposomes with different DOPC:DOPS ratios. (a) SH scattering patterns recorded in the PPP polarization combination. (b) SH scattering patterns recorded in the PSS polarization combination. The polarization ratios report on outgoing (first letter) and incoming (last two letters) beams with P(S) indicating a parallel (perpendicular) polarization with respect to the horizontal scattering plane. The lines represent fits made with the nonlinear Rayleigh-Gans-Debye theory[13] using the parameters of Table I. The surface potential values were extracted from the fits and are plotted in Fig. 4. (c) Maximum SH intensity as a function of DOPS weight percentage in the liposomes (recorded in the PPP polarization combination).

$\Phi_0 = -145 \pm 30$ mV (pure DOPS). The obtained values for Φ_0 are plotted in Fig. 4(a).

The maximum magnitude for Φ_0 is reached at ~10 *w/w* % of DOPS in the liposomes. The values for Φ_0 can be compared to ζ-potential values (Fig. 4(b)) that were extracted from the electrophoretic mobility measurements of the same samples using Smoluchowski's approximation. The ζ-potential follows the same trend as the surface potential: The magnitude of the ζ-potential increases with increasing DOPS concentration and levels off at ~10% DOPS. At higher concentrations, the ζ-potential remains constant at −44 ± 7 mV, independent of the DOPS concentration.

The saturated values of Φ_0 and ζ differ significantly, by ~100 mV. This difference offers an opportunity to obtain some insight into the molecular level structure of the interfacial layer. To estimate the behavior of the electrostatic potential and the amount of free charges on the DOPS head groups, we need to assume a model for the structure of the interfacial region. Assuming an arbitrary sized smooth sphere with a certain surface charge density σ_0 that is embedded in a continuous medium with a 1:1 electrolyte concentration (c), we can compute both the surface charge density σ_0 and the decay of the electrostatic potential into the solution $\Phi(r)$ for a given value of Φ_0. Using Ohshima's exact solution for the potential distribution around a sphere with arbitrary potential (also known as the spherical Gouy-Chapman model), we have[26]

$$\Phi(r) = \frac{2k_BT}{ze} \ln\left[\frac{1+\tanh\left(ze\Phi_0/4k_BT\right)(R/r)\,e^{(-\kappa(r-R))}}{1-\tanh\left(ze\Phi_0/4k_BT\right)(R/r)\,e^{(-\kappa(r-R))}}\right] \quad (4)$$

and

$$\sigma_d = \frac{2\varepsilon_0\varepsilon_r\,\kappa\,k_BT}{e}\sinh\left(\frac{ze\Phi_0}{2k_BT}\right)\times\left[1+\frac{1}{\kappa R}\frac{2}{\cosh(ze\Phi_0/4k_BT)^2} + \frac{1}{(\kappa R)^2}\frac{8\ln[\cosh(ze\Phi_0/4k_BT)]}{\sinh(ze\Phi_0/2k_BT)^2}\right]^{1/2} \quad (5)$$

with $\varepsilon_0, \varepsilon_r, k_B, T, z, e, \kappa, R$ being the permittivity in vacuum and the relative permittivity, the Boltzmann constant, Temperature, valency, elementary charge, Debye parameter and the radius of the liposome. Figure 4(c) shows the computed potential decay using Eq. (4) (dashed blue curve). The ζ-potential is also indicated in the graph. The ζ-potential is the potential that is measured at the boundary between stagnant and free flowing liquid (the shear or slipping plane, positioned at a distance d away from the surface).[15,27] This plane is thought to be positioned not more than ~3 water diameters (<~1 nm) away from the interface of an atomically smooth surface. In our samples, there will be some variations in the positions of the lipids as they are in the liquid phase and exhibit thermal motion so that the liposome surface is not atomically smooth. This could lead to variations on the order of ~1 nm, but certainly not more.[28] Applying Eq. (4) to the found values of Φ_0 and determining where the $|\zeta|$-potential

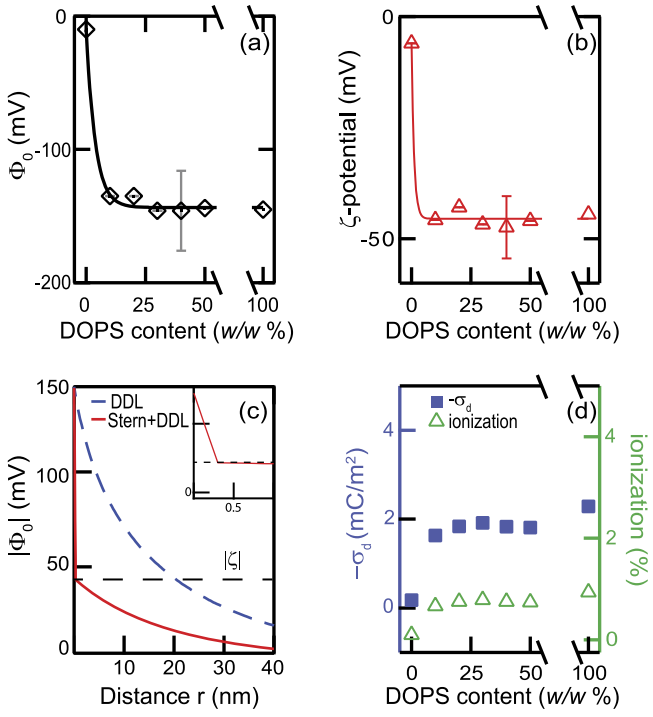

FIG. 4. Surface and ζ-potential of liposomes with different DOPC:DOPS ratios. (a) Extracted surface potential values from the data fits of Figs. 3(a) and 3(b). (b) ζ-potential values for the same samples as in panel (a) using the Smoluchowski approximation. The error bars represent the standard deviations from 75 measurements. Solid lines are guides to the eye. (c) Computed values for the electrostatic potential as a function of distance (r, at r = 0, r = R) along the surface normal for a diffuse double layer only (labeled DDL, dashed blue curve) and a Stern layer with a diffuse double layer (solid red curve). The inset shows a zoom-in for 0 < r < 1 nm. (d) The computed surface charge density σ_d at the shear plane (solid blue squares) and the overall degree of ionization (open green triangles) of the liposomes as a function of DOPS content.

crosses the Φ_0(r)-curve result in a slipping plane distance of d = 20 nm. This is physically unreasonable: It does not seem energetically meaningful to have a layer of 60 stagnant water molecules. According to the above mentioned criteria, the slipping plane should be at a maximum distance d < 2 nm. The potential difference $|\Phi_0 - \zeta|$ then should occur over a distance d < 2 nm, which requires a significant electrostatic field strength of $>4.9{\cdot}10^7$ V/m. In case d = 0.3 nm (which corresponds to one layer of water molecules and is the lower limit of the slipping plane distance[29,30]), the field strength becomes $3{\cdot}10^8$ V/m. If an electrostatic field with such a high strength emerges from the surface, it will result in a high concentration of counter-ions. This hints towards a low degree of completely ionized surface head groups and the presence of a Stern-like or charge condensation layer when the DOPS concentration exceeds 10%, even though the ionic strength of the solution is low. With that expectation in mind, the potential distribution from the shear plane into the bulk solution should be modified by replacing Φ_0 with ζ. The resulting estimated distance dependent potential is plotted in Fig. 4(c) considering a linear decay as in a planar constant capacitor model.[27,31] The charge density σ_d on the shear plane is then determined by Eq. (5) using ζ instead of Φ_0. Values for σ_d (solid blue squares, left axis) and the corresponding degree of ionization on the liposomes (σ_d/σ_0, open green triangles, right axis) are plotted in Fig. 4(d). For this calculation, we used a σ_0 calculated using effective head group areas[17] that range between 0.653 nm^2 and 0.713 nm^2 for DOPS and DOPC:DOPS [9:1] liposomes (Table I). The degree of ionization as calculated at the shear plane is almost constant around 1% indicating that almost all charges are screened within the first few hydration shells. Note that for 100% DOPS liposomes, this means that only 1 in 100 DOPS molecules have no counter-ions associated with them, and for liposomes with 10% DOPS, this amounts to ~1 in 10 lipids. Such a degree of counter-ion condensation at the outer leaflet would require a total effective interfacial Na^+ concentration that is on the order of 1–3M (assuming the lipid head group area and thickness of the condensed layer as mentioned above). Note that the inner leaflet is charge neutral as required from fundamental electrostatics considerations.[12]

The observed large difference between the two determined potentials and the independence of the surface and ζ-potential on the surface charge density are clear indicators of some form of charge condensation at the outer leaflet of the liposomes. Charge condensation[32] is more commonly observed in polyelectrolyte solutions (Ref. 33 and references therein) and some colloidal systems.[34,35] It occurs in solutions of low ionic strength as a consequence of free energy minimization that involves both electrostatic (enthalpic) interactions that favour association and entropic interactions that tend towards dissociation.[36] For spherical particles with radii (R) that are comparable in size to the Debye length ($1/\kappa, \kappa R \sim 1$), the critical surface charge density ($\sigma_{0,crit}$) above which charge condensation occurs is[36]

$$\sigma_{0,crit} = \frac{e(1+\kappa R)\ln(\kappa l_b)}{2\pi R z l_b}, \tag{6}$$

where κ is the Debye screening parameter ($\kappa = \sqrt{\frac{2000e^2z^2N_Ac}{\epsilon_0\epsilon_r k_B T}}$, c the respective concentration, R the radius of the liposome, l_b the Bjerrum length in water (0.71 nm), and z the valency (1). For the liposome solutions, we obtain $-7.9 < \sigma_{0,crit} < -6.7$ mC/m^2. A theoretical maximum surface charge density for complete ionization of 100% (10%) DOPS liposomes would be $\sigma_0 = -245$ mC/m^2(-22.5 mC/m^2) considering 1 charge per head group and the same head group areas as before. Our surface charge density is thus much larger than the computed critical value above which charge condensation occurs. Based on Eq. (6), we can infer that condensation would start at around 3% of DOPS in the liposome, which is in reasonable agreement with our data considering the error bars.

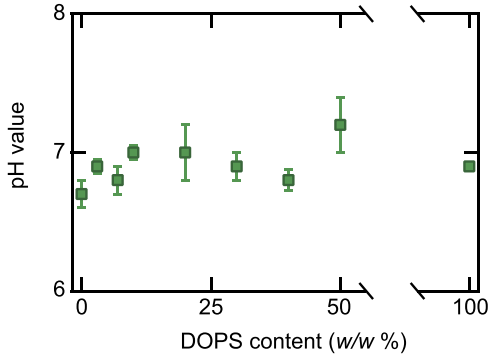

FIG. 5. Variation in the bulk pH of DOPC:DOPS liposome solutions. The pH was derived from three consecutive potentiometric measurements. Error bars indicate the standard deviation of at least three measurements.

A question one might ask is if the counter-ions that are responsible for the charge condensation consist of Na^+ ions or H^+ ions from the autoprotolysis reaction of water. If H^+ is responsible for the condensation of charge, given the amount of charge condensation (~99%) and the number of liposomes in the solution (~2.87×10^{12} liposomes cm^{-3}) for the liposomes with 100% DOPS, we may expect a change of the bulk pH value to pH = 10.4. A potentiometric measurement of the pH as a function of DOPS concentration did not show any changes (Fig. 5). As such the condensed layer most likely consists of Na^+ ions.

IV. CONCLUSIONS

In conclusion, we characterized DOPC:DOPS liposomes with polarimetric AR-SHS as a function of lipid composition and size. The polarization state resolved AR-SHS response is an indicator for the amount of orientationally ordered water which is used to extract the membrane surface potential. As the DOPS membrane content is varied from 0% to 100%, the surface potential changes from −10 to −145 mV at a few percent of DOPS in the membrane after which it remains constant. The ζ-potential shows the same trend but has a drastically lower saturation value (−44 mV). The big potential difference and the absence of sensitivity of both potentials on the amount of charged lipids in the membrane are explained by the formation of a condensed layer of Na^+ counter-ions around the liposome. This explanation agrees well with the predictions of charge condensation theory for polyelectrolyte systems.

The presented experimental findings demonstrate that the Gouy-Chapman model, despite its wide use,[37–41] is not

suitable without modification to describe the diffuse double layer around lipid membranes, even under conditions of low ionic strength. Specifically, the relatively strong association of counter-ions with interfacial charged groups should be taken into account. In addition, from a purely theoretical perspective, there is still an ongoing discussion about the ion behavior at charged interfaces at high concentrations, for which different scenarios from simulations exist,[42] but also at low concentrations, for which very little data exist. The presented data will help select the correct way to describe theoretically the composition and physical chemistry of membranes in terms of ion distribution.

ACKNOWLEDGMENTS

This work is supported by the Julia Jacobi Foundation and the European Research Council (Grant No. 240556).

[1] M. H. Abraham, G. S. Whiting, R. Fuchs, and E. J. Chambers, J. Chem. Soc., Perkin Trans. **2**, 291 (1990).
[2] L. Schneider, H. J. Schmid, and W. Peukert, Appl. Phys. B **87**, 333 (2007).
[3] S. Roke and G. Gonella, Annu. Rev. Phys. Chem. **63**, 353 (2012).
[4] B. Schürer, S. Wunderlich, C. Sauerbeck, U. Peschel, and W. Peukert, Phys. Rev. B **82**, 241404 (2010).
[5] B. Schürer and W. Peukert, Part. Sci. Technol. **28**, 458 (2010).
[6] R. Scheu, Y. Chen, H. B. de Aguiar, B. M. Rankin, D. Ben-Amotz, and S. Roke, J. Am. Chem. Soc. **136**, 2040 (2014).
[7] Y. X. Chen, K. C. Jena, C. Lütgebaucks, H. I. Okur, and S. Roke, Nano Lett. **15**, 5558 (2015).
[8] R. Scheu, Y. Chen, M. Subinya, and S. Roke, J. Am. Chem. Soc. **135**, 19330 (2013).
[9] Y. Liu, E. C. Y. Yan, X. Zhao, and K. B. Eisenthal, Langmuir **17**, 2063 (2001).
[10] N. Smolentsev, C. Lütgebaucks, H. I. Okur, A. De Beer, and S. Roke, J. Am. Chem. Soc. **138**, 4053 (2016).
[11] C. Lütgebaucks, G. Gonella, and S. Roke, Phys. Rev. B **94**, 195410 (2016).
[12] J. D. Jackson, *Classical Electrodynamics* (Wiley, New York, 1999).
[13] G. Gonella, C. Lütgebaucks, A. G. F. de Beer, and S. Roke, J. Phys. Chem. C **120**, 9165 (2016).
[14] G. van Meer, D. R. Voelker, and G. W. Feigenson, Nat. Rev. Mol. Cell Biol. **9**, 112 (2008).
[15] R. J. Hunter, *Zeta Potential in Colloid Science* (Academic Press, Sydney, 1981).
[16] P. S. Chen, T. Y. Toribara, and H. Warner, Anal. Chem. **28**, 1756 (1956).
[17] H. I. Petrache, S. Tristram-Nagle, K. Gawrisch, D. Harries, V. A. Parsegian, and J. F. Nagle, Biophys. J. **86**, 1574 (2004).
[18] C. Gardiner, M. Shaw, P. Hole, J. Smith, D. Tannetta, C. W. Redman, and I. L. Sargent, J. Extracell. Vesicles **3**, 25361 (2014).
[19] N. Gomopoulos, C. Lutgebaucks, Q. C. Sun, C. Macias-Romero, and S. Roke, Opt. Express **21**, 815 (2013).
[20] J. I. Dadap, J. Shan, K. B. Eisenthal, and T. F. Heinz, Phys. Rev. Lett. **83**, 4045 (1999).
[21] A. G. F. de Beer and S. Roke, J. Chem. Phys. **132**, 234702 (2010).
[22] S. Roke, M. Bonn, and A. V. Petukhov, Phys. Rev. B **70**, 115106 (2004).
[23] A. V. Gubskaya and P. G. Kusalik, Mol. Phys. **99**, 1107 (2001).
[24] J. I. Dadap, J. Shan, and T. F. Heinz, J. Opt. Soc. Am. B **21**, 1328 (2004).
[25] A. G. F. de Beer, R. K. Campen, and S. Roke, Phys. Rev. B **82**, 235431 (2010).
[26] H. Ohshima, *Theory of Colloid and Interfacial Phenomena* (Academic Press, Tokyo, 2006).
[27] J. Lyklema, *Fundamentals of Interface and Colloid Science: Liquid-Fluid Interfaces* (Academic Press, Wageningen, 2000).
[28] S. Y. Bhide and M. L. Berkowitz, J. Chem. Phys. **123**, 224702 (2005).
[29] J. T. Davies and E. K. Rideal, *Interfacial Phenomena* (Academic Press Imprint Elsevier Science & Technology Books, San Diego, 1963).
[30] R. J. Hunter, *Foundations of Colloid Science* (Oxford University Press, 2001).
[31] P. C. Hiemenz and R. Rajagopalan, *Principles of Colloid and Surface Chemistry* (Marcel Dekker, New York, 1997).
[32] G. S. Manning, J. Chem. Phys. **51**, 924 (1969).
[33] G. S. Manning, Eur. Phys. J. E **34**, 39 (2011).
[34] U. Böhme and U. Scheler, Adv. Colloid Interface Sci. **158**, 63 (2010).
[35] D. A. J. Gillespie, J. E. Hallett, O. Elujoba, A. F. Che Hamzah, R. M. Richardson, and P. Bartlett, Soft Matter **10**, 566 (2014).
[36] G. S. Manning, J. Phys. Chem. B **111**, 8554 (2007).
[37] M. R. Moncelli, L. Becucci, and R. Guidelli, Biophys. J. **66**, 1969 (1994).
[38] D. H. Mengistu, E. E. Kooijman, and S. May, Biochim. Biophys. Acta, Biomembr. **1808**, 1985 (2011).
[39] M. Yi, H. Nymeyer, and H.-X. Zhou, Phys. Rev. Lett. **101**, 038103 (2008).
[40] S. McLaughlin, Annu. Rev. Biophys. Biophys. Chem. **18**, 113 (1989).
[41] J. M. Troiano *et al.*, J. Phys. Chem. C **119**, 534 (2015).
[42] N. Agmon, H. J. Bakker, R. K. Campen, R. H. Henchman, P. Pohl, S. Roke, M. Thämer, and A. Hassanali, Chem. Rev. **116**, 7642 (2016).